https://doi.org/10.5194/nhess-2022-295
Preprint. Discussion started: 10 January 2023

Natural Hazards and Earth System Sciences
Discussions

More than one landslide per road kilometer – surveying and modelling mass movements along the Rishikesh-Joshimath (NH-7) highway, Uttarakhand, India

Jürgen Mey[1], Ravi Kumar Guntu[2], Alexander Plakias[1], Igo Silva de Almeida[1], Wolfgang Schwanghart[1]

[1]Department Institute of Environmental Science and Geography, University of Potsdam, Potsdam-Golm, 14476, Germany
[2]Department of Hydrology, IIT Roorkee, Roorkee, 247667, India

Correspondence to: Jürgen Mey (juemey@uni-potsdam.de)

Abstract. The rapidly expanding Himalayan road network connects rural mountainous regions. However, the fragility of the landscape and poor road construction practices lead to frequent mass movements along-side roads. In this study, we investigate fully or partially road-blocking landslides along the National Highway (NH-) 7 in Uttarakhand, India, between Rishikesh and Joshimath. Based on an inventory of >300 landslides along the ~250 km long corridor following exceptionally high rainfall in October and September 2022, we identify the main controls on the spatial occurrence of mass-movement events. Our analysis and modelling approach conceptualizes landslides as network-attached spatial point pattern. We evaluate different gridded rainfall products and infer the controls on landslide occurrence using Bayesian analysis of an inhomogeneous Poisson process model. Our results reveal that slope, rainfall amounts, and lithology are the main environmental controls on landslide occurrence. The individual effects of aggregated lithozones is consistent with previous assessments of landslide susceptibilities of rock types in the Himalayas. Our model spatially predicts landslide occurrences and can be adapted for other rainfall scenarios, and thus has potential applications for efficiently allocating efforts for road maintenance. To this end, our results highlight the vulnerability of the Himalayan road network to landslides. Climate change and increasing exposure along this pilgrimage route will likely exacerbate landslide risk along the NH-7 in the future.

1 Introduction

Roads are at the heart of the Himalayan transport infrastructure. They are vital for national and international trade and passenger movement, and strategically important in border areas. India has improved and expanded its road network in mountainous states under the national Bharatmala Pariyojana ("Road to Prosperity") initiative, established in 2015. Key objectives of this highway development program are to improve the efficiency and connectivity of the transport infrastructure and to provide road access to remote border regions and rural areas. Yet, in mountainous environments, roads are exposed to various degrading processes. Among these processes, mass movements particularly inflict severe structural damage and heavily degrade road serviceability (Meyer et al., 2015). Traffic disruptions due to mass movements can have severe consequences, if they impede accessibility and compromise rescue operations during extreme events such as cloudbursts, floods and earthquakes. Ensuring accessibility and connectivity thus requires considerable maintenance efforts (Uniyal, 2021).

According to the National Crime Records Bureau (2022), 160 people died due to landsliding in Uttarakhand in the last four years. These figures exclude other extreme events like heavy rainfalls, floods or the 2021 Chamoli rock and ice avalanche with over 200 fatalities (Shugar et al., 2021). Several studies have addressed mass movements and their relation to transport infrastructure in the Indian and Nepal Himalayas. The studies range from purely phenomenological descriptions (e.g., Bartarya & Valdiya, 1989; Sarkar & Kanungo, 2006), to statistical (Das et al., 2012; Devkota et al., 2013; Sur et al., 2020) and physically based modelling approaches (e.g., Kanungo et al., 2013; Prasad & Siddique, 2020). In fact, the space limitation in steep terrain often requires road construction to undercut slopes beyond their angle of repose, reducing slope stability and increasing landslide susceptibility (e.g., Barnard et al., 2001; Haigh & Rawat, 2011; Li et al., 2020). Therefore, particular attention has focused on detailed stability assessments of road cut slopes (e.g., Kundu et al., 2016; Siddique et al., 2017; Siddique & Pradhan, 2018; Singh et al., 2014) and the development of appropriate remedial measures (e.g., Adhikari et al., 2020; Asthana & Khare, 2022; Koushik et al., 2016; Rawat et al., 2016), but fewer studies have attempted to predict the spatial occurrence of mass movements along roads. Knowledge about where and when landslides preferably detach is important for early warning but also for efficiently allocating efforts of road maintenance and slope enforcements (Haigh, 1984). Using data on occurrences of landslides, susceptibility studies aim to quantify the spatial propensity of hillslopes to fail and to determine the controlling factors such as terrain attributes e.g., slope angle and aspect, and geo-environmental variables e.g., rainfall intensity and lithology.

In this study we carry out a landslide susceptibility analysis for a ~250 km long stretch of the National Highway 7 (NH-7) that connects the cities of Rishikesh and Joshimath, Uttarakhand, India (Fig.1). We conducted a detailed survey of partially or fully road-blocking landslides along the road following a period of intense rainfalls in September and October 2022. In contrast to previous studies, which focused on the spatial prediction of landslides in two spatial dimensions, our analysis and modelling approach conceptualizes landslides as network-attached spatial point pattern (Baddeley et al., 2021). One of the critical covariates in our modelling approach is the spatial distribution of accumulated rainfall amounts. We thus evaluate different rainfall products. Finally, we infer the controls on landslide occurrence using Bayesian analysis of multivariate loglinear models. We present our results and discuss uncertainties and potential shortcomings of our approach. We conclude with recommendations for refinement of the approach and further research avenues.

https://doi.org/10.5194/nhess-2022-295
Preprint. Discussion started: 10 January 2023

Natural Hazards and Earth System Sciences
Discussions

2 Study site

The NH-7 ascends from 400 m at Rishikesh to approximately 2000 m at Joshimath, crossing steep terrain with soil mantled slopes that range in inclination from 20° to 40°. Mean annual rainfall (1970–2019) varies from 1500–2000 mm around Rishikesh to 1000–1200 in Joshimath with 80–86 % and 60–70 % delivered by the Indian summer monsoon (June to September), respectively (Pai et al., 2014; Swarnkar et al., 2021). Air temperature in Rishikesh is always above freezing and ranges between 4 and 40 °C, whereas the temperature in Joshimath varies between -10 and 20 °C. This climatic gradient is reflected in a gradual change in vegetation. Accordingly, in the lower lying subtropical region dense deciduous forest dominates, which is replaced by a temperate broadleaf mixed forest and temperate shrub and grassland communities where forest has not been preserved.

The geological framework of the study area is largely determined by the ongoing Indo–Asian collision that causes crustal thickening and exhumation along large-scale detachment zones and thrust faults. Most of the study area lies within the Lesser Himalaya, between the Main Boundary Thrust in the south and the Main Central Thrust in the north, which are splays of the root detachment, the Main Himalayan Thrust (Figure 1). As the present-day India–Eurasia convergence is on the order of 36–40 mm yr^{-1} (e.g., Wang et al., 2001) and approximately half of this is accommodated within the Himalayas (e.g., Lavé & Avouac, 2000), the region is seismically active and bears the potential for large earthquakes (e.g., Kayal et al., 2003; Bollinger et al., 2014; Rajendran et al., 2017).

The highway runs perpendicular to the strike of the orogen and crosses rocks of the Lesser Himalayan Sequence (LHS) and the High Himalayan Crystalline (HHC) that represent the ancient passive Indian margin, and which are separated by the Main Central Thrust (MCT). The LHS is mainly composed of sedimentary and low-grade metasedimentary rocks; quartzite, shale, phyllites and slate with occasional limestone and dolomite, whereas the HHC is characterized by high-grade schist, gneiss and quartzite. These rocks feature a high density of discontinuities like faults, fractures and joints that are important seepage pathways. In locations, where the road cuts through weathered rocks and intersects with major faults, the hillslopes are particularly fragile (Prasad & Siddique, 2020).

During the week before we conducted our survey, almost the entire Indian north experienced a strong positive rainfall anomaly. The state of Uttarakhand registered a departure of 1040 % from the average. The districts of Tehri Garhwal, Pauri Garhwal, Rudraprayag and Chamoli, through which the NH-7 runs, recorded a weekly surplus of 419 %, 679 %, 218 % and 1855 %, respectively (https://mausam.imd.gov.in/imd_latest/contents/rainfall_statistics_2.php, supplementary data). Given that the mean monthly rainfall in October is around 35 mm, approximately three times the monthly average rainfall occurred in only one week, which is close to the rate that prevails during the monsoon.

https://doi.org/10.5194/nhess-2022-295
Preprint. Discussion started: 10 January 2023

The NH-7 is a lifeline for socioeconomic development which is mainly based on agriculture, trade, tourism, mining and hydropower. Furthermore, the highway is vital for the Indian military to transport personnel and equipment to their outposts up to the Indian/Chinese-Tibetan border. During the pilgrimage season (May – Oct) more than one million people visit the holy shrines of Badrinath and Kedarnath using this highway. Moreover, as it follows the course of the Ganges and its tributary Alaknanda, the road passes the river confluences known as the five Prayags, namely Devprayag, Rudraprayag, Karnaprayag, Nandaprayag and Vishnuprayag (Fig. 1). In Hinduism these confluences are considered sacred and attract pilgrims to bathe in the flows before worshiping the rivers. Finally, there are ten hydroelectric power plants within 20 km distance to the road and numerous more are planned or are under construction, highlighting the road's importance in terms of energy security and economic value.

3 Methods

Travelling to fieldwork in the Chamoli area on Oct 15, 2022, we recognized numerous, partially road-blocking landslides along the road. We thus spontaneously decided to inventory these landslides as road workers already began to clean the road from the debris, thus rapidly removing evidence of smaller landslides that detached in close vicinity to the road. We mapped landslides along the road both on our way towards Chamoli on Oct 15 and 16, as well as on our way back on Oct 18, 2022. We used handheld GPS devices to map the locations at which landslides intersected with the road between Rishikesh and Joshimath, Uttarakhand (Figure 1). We only mapped landslides with runouts affecting the road, thus partially or fully blocking it (Figure 2). We considered partial blockages as those where the emplaced deposits either substantially narrowed the road, or, if the road was marked, marginal strips were crossed by the debris. Very small landslides with an area of less than ~10 m^2 were not considered. We checked each landslide location using Google Earth using the latest and historic imagery and classified each location as (1) new landslide, (2) road-blocking landslide visible before the Sep–Oct 2022 rainfall anomaly, and (3) reactivated landslide. We assigned the last category to those landslides where a slip surface and scar were well-identifiable in the imagery. This was not always straightforward since landslide scars cannot always be clearly distinguished from unvegetated engineered slopes and road widening.

We conceptualize landslides along the road as network-attached spatial point process. A spatial point process is a stochastic mechanism, which controls the spatial distribution of events or occurrences (Baddeley et al., 2015). As our mapped landslides are events that occur along the road – and only these have been mapped – these events are constrained to lie on a network of lines (Baddeley et al. 2021, Okabe et al. 2006). In our case, the network is rather simple as it consists of only one polyline, but we emphasize that our approach can be extended to more complicated network topologies.

We use TopoToolbox (Schwanghart and Scherler, 2014) and its numerical object PPS (Schwanghart et al., 2021) to analyze, visualize, and model the density of landslides along the road. PPS has been designed to work with point patterns on stream networks, but it can be applied to dendritic, undirected networks of any kind. The numerical approach consists of a fine-pixel approximation which is controlled by the geometry of the digital elevation model (DEM) from which the data is retrieved. This means that the vector shape of the road is pixelated with the same geometry as the DEM (Schwanghart et al., 2021). We model landslide densities with an inhomogeneous Poisson process, which is described by its intensity function $\lambda(u)$ with u being the horizontal distance along the road. A common parametric model of the intensity is the loglinear model:

$$\boldsymbol{\lambda}(\boldsymbol{u}) = \exp(\beta_0 + \boldsymbol{\beta X}), \quad (1)$$

where $\boldsymbol{X}$ is a matrix of predictor variables (covariates), β_0 is an intercept and $\boldsymbol{\beta}$ is a vector of model parameters**.** A key property of the model is that the events are independent from each other. Spatial dependence of events can occur in different ways leading to clustering, i.e., points tend to occur close to other points, or inhibition, i.e., there is a characteristic distance or regularity in the spacing between the points. Spatial clustering of landslide events has previously been addressed by Lombardo et al. (2018, 2019) using a Cox Process model to emulate the latent spatial effects of unobserved variables, whereas inhibition can be observed, for example, in data where areal non-overlapping phenomena are represented as points (Evans, 2012; Schwanghart et al., 2021). At this stage, we will not include these potential second-order effects on the density of landslides, but we will investigate their possibility using the inhomogeneous K-function defined by Ang et al., (2012) once we have modelled first-order effects.

We use following candidate predictor variables in the loglinear model introduced above. First, we hypothesize that steep hillslopes gradients next to the road are more susceptible to mass wasting events. Based on the Copernicus 30 m DEM (European Space Agency, 2021), we thus calculate surface gradients. We identify those areas that lie right or left to the road, and which are higher than the road itself within a buffer zone of ~210 m (or 7 pixels). We identify the nearest DEM pixels and map the mean gradients of these nearest pixels to the road network. These values vary greatly over short distances and thus we smooth them using the algorithms (with smoothness penalty parameter K = 5) described by Schwanghart and Scherler (2017). Next to gradient, we consider that rainfall patterns exert a strong influence on the occurrence of landslides. We consider five rainfall products (see Table 1) to comprehend the rainfall patterns from various perspectives. IMD1 solely takes into account gauge-based measurements from a network of stations provided by the Indian Meteorological Department (Pai et al., 2014). Gauge measurements and IMERG final run estimates are merged in IMD2 (Mitra et al., 2009). MSWEP v2 is another merged product that incorporates reanalysis-based, gauge, and satellite-derived rainfall estimates (Beck et al., 2017). CHIRPS v2 provides a high-resolution record by combining gauge and satellite data from NOAA (National Oceanic and Atmospheric Administration) (Funk et al., 2015). The Japan Aerospace Exploration Agency developed the GSMaP dataset by blending multi-satellite rainfall estimations (Kubota et al., 2007). We resample the rainfall grids to the resolution of the DEM and extract the values for each road pixel. Finally, we obtained a digitized version of the lithology of

https://doi.org/10.5194/nhess-2022-295
Preprint. Discussion started: 10 January 2023

Uttarakhand in the scale of 1:2M, from the Geological Survey of India (2022). The data contains both stratigraphic as well as lithological information. Accordingly, the NH-7 crossed 34 different lithologies along the stretch from Rishikesh to Joshimat. To reduce the number of potential categories, we summarized and aggregated the lithological information into lithozones with less focus on the stratigraphic context. This simplification resulted in five lithozones that are dominated by carbonate rocks (1), phyllite and shale (2), quartzite (3), quartzite and igneous rocks (4) and crystalline high grade metamorphics (5). The reclassification is shown in Table 2. Again, we gridded this data and assigned corresponding lithozones to each road pixel.

We adopt a Bayesian strategy to infer and identify predictor variables using the function bayesloglinear of the PPS numerical class (Schwanghart et al., 2021). The function provides an interface to bayesreg (Makalic and Schmidt, 2016), a MATLAB toolbox that enables efficient Bayesian modelling and regularization of high-dimensional data. We use a Bayesian lasso estimator with Laplace prior distributions for the regression coefficients. The sampling creates 1000 burnin samples before calculating 1000 posterior samples. To avoid autocorrelation of the posterior samples, we use a level of thinning of five samples. To this end, we find that 1000 samples are sufficient to characterize the posterior distributions.

Finally, we evaluate the model based on the Receiver-Operating Characteristics (ROC) Area under the Curve (AUC) approach. We visualize the predictions and inspect and analyze spatial densities obtained from random realizations of the fitted inhomogeneous Poisson process model. In addition, we test whether additional covariates provide opportunities for further improving the model. The selected attributes include terrain roughness and total curvature as well as land cover derived from the Copernic Global Land Operations (CGLOPS-1, Moderate dynamic land cover 100 m, version 3) (Buchhorn et al., 2020), which we reclassify according to Table 3. We investigate these models using a frequentist modelling approach (see PPS-function fitloglinear) and compare models with additional covariates with the Akaike Information Criterion (AIC).

4 Results

We recorded 309 fully or partially road-blocking landslides along the 247 km long road between Rishikesh and Joshimath (Figure 1) which amounts to an average landslide intensity of 1.25 landslides per km. The average nearest distance between adjacent landslides is 315 m which demonstrates that the points are unevenly distributed along the road. A two-sample Kolmogorov-Smirnoff test between the road distance (uniform distribution between start and end of the surveyed road), and the road distances measured at the landslides rejects the null hypothesis with $p \approx 0$ that landslide locations follow a completely spatial random distribution. Yet not all field-mapped landslide occurrences can be attributed to the anomalously high rainfall period during September and October 2022. Visually inspecting the locations using Google Earth reveals that 21.4 % of the recorded landslides with road blockages existed before (Figure 1). 17.8 % of the landslides were most likely reactivated by the excessive rainfall because they could not be identified to be road-blocking before the rainfall period. Most

https://doi.org/10.5194/nhess-2022-295
Preprint. Discussion started: 10 January 2023

landslides (60.8 %) were not identifiable as such in the Google Earth imagery available for several dates before and including March 2022.

The spatial distribution and amounts of accumulated rainfall during September and October 2022 differ between the rainfall products (Figure 3). Since independent measurements based on rain gauges are unavailable, we investigate the performance of the rainfall products to explain the spatial distribution of landslides. The approach uses the AIC to iteratively evaluate models including one of the rainfall products at a time, as well as hillslope gradient and lithozones. AIC values vary between 1886 and 1916 with CHIRPS v2 having the lowest AIC. GSMaP also correlates positively with landslide density, but less than CHIRPS v2, whereas IMD1, IMD2 and MSWEP show no significant correlation. We thus use CHIRPS v2 in the development of the subsequent models. We emphasize that including different rainfall products in the model has no strong effect on the remaining model parameters that determine the influence of slope and lithozones. In other words, the choice of rainfall product does not affect our results and conclusions about the topographic and lithologic controls on landslide occurrence.

Bayesian loglinear modelling of the landslide density (Figure 4, Figure 5a, b) reveals a credible influence of the covariates rainfall (Figure 5c), slope (Figure 5d), and lithozones (Figure 5e) (see Figure 4 for posterior means and 95 % highest density intervals and Figure 6 for individual effects). A Bayesian feature rank algorithm based on the absolute magnitude of the parameters in each posterior sample (Makalic and Schmidt, 2011) ranks slope as the top covariate in terms of explanatory power, followed by rainfall and lithozones. Among the lithozones, zones 4 and 2 stand out as important categories improving the explanatory power of the model. The individual effects of the covariates reveal a positive influence of rainfall and slope on landslides (Figure 6a, b). Predictions of landslides densities in lithozone 4 are credibly lower than in lithozone 2 given equal rainfall and slope. The spatial pattern of predicted landslide density (Figure 5f) is consistent with observed spatial density variations, but the higher variability reflects the importance of slope as predictor variable.

The AUC is an aggregated metric for a point pattern model across thresholds and ranges between 0.5 and 1. Our loglinear model has an AUC value of 0.76 (Figure 7a). The inhomogeneous K-function shown in Figure 7b quantifies the expected number of points as a function of distance from each point, adjusted for the modelled inhomogeneous intensity of the point pattern. Distances between individual landslides are calculated as the shortest-path distance along the road rather than the direct Euclidean distance. Acceptance intervals around the theoretical K function derive from repeated simulations of the inhomogeneous Bayesian loglinear model. The actual point pattern’s K function is outside these acceptance intervals, suggesting a clustering that cannot be explained by the covariates. A comparison of 100 randomly simulated and actual point densities (Figure 7c) shows that the modelled and observed spatial landslide densities are consistent although the second, smaller peak of landslide densities close to Joshimath are not well captured by the model.

Can the model be improved by incorporating more explanatory covariates? Our impression in the field was that landslides detach independently of planform hillslope geometry as they occurred both on spurs and convex hollows. Nevertheless, we calculated total curvature and topographic roughness as potential predictor candidates. In addition, we used landcover (Table 3) and distance to faults (Figure 1) as they are commonly used in susceptibility studies (e.g., Stanley and Kirschbaum 2017, Li et al., 2020, Ozturk et al., 2021). All in all, these metrics barely contribute to improving the model fit and their incorporation in the model would, according to the AIC, lead to overfitting (Figure 8).

5 Discussion

We recorded more than one landslide per road kilometer along the NH-7 highway between Rishikesh and Joshimath. The fact that this road is strongly affected by landslides has been previously described and attributed to the region's fragility of slopes, focused rainfall and frequent seismicity (Sati et al., 2011). In addition to the environmental conditions, road construction and widening have contributed to the formation of new landslides which are often shallow and small, but which nevertheless inflict fatalities, severe damages to infrastructure and traffic disruption (Sati et al., 2011). We conducted a systematic survey of landslides and derived a statistical model that aims at quantifying landslide susceptibility along the NH-7 at a high spatial resolution.

Our analysis relied on a GPS-based survey of landslides while travelling from Rishikesh to Joshimath shortly after a period of anomalously high rainfall. Using this approach, we mapped landslides irrespective of cloud cover and without acquiring high-resolution satellite imagery which is needed to detect small landslides. A drawback, however, is that we may have missed landslides where debris had already been removed by road works. Also, detailed mapping of the areal extent of the landslides was not possible during drive-by so that we did not quantify the size of landslides. Thus, our modelling approach treats all landslides the same, irrespective of their areal extent and volume. To this end, however, this enables us to adopt a modelling approach which conceptualizes landslides as unmarked network-attached point pattern (Baddeley et al., 2021; Okabe and Sugihara, 2012). Representing landslides as network-attached points and not as areal features entails advantages and disadvantages. Constraining landslide locations to lie on roads demands that all predictor variables also need to be mapped to the road network, which entails some generalization and additional degrees of freedom about the choice and aggregation of 2D variables. For landslide susceptibility analysis, for example, this means that spatial variables characterizing the source area (e.g., hillslope gradient) are projected onto the road. At the same time, model development and fitting benefits from smaller sample sizes as data amounts are moderate and computational demands during Bayesian posterior sampling remain manageable.

We detected a profound difference between rainfall products, for which a detailed analysis is outside the scope of this study. These differences have been recognized before by several studies along the Himalayan orographic front and have either been

https://doi.org/10.5194/nhess-2022-295
Preprint. Discussion started: 10 January 2023

attributed to the network of rain gauges, which is particularly sparse at high elevations, or, if rainfall estimates are based on remote sensing data, to irregular return times, owing to which individual rainfall events may be missed (Andermann et al., 2011, Hu et al., 2016). To this end, these uncertainties are crucial for capturing the spatial patterns of landslides (Ozturk et al., 2021). We found that CHIRPS v2 performed best in predicting the spatial landslide patterns along NH-7 but the employed search strategy must be viewed critically as the reverse conclusion, that landslides are controlled by these patterns is not necessarily true. Indeed, studies come to different conclusions about the performance of CHIRPS v2 and other gridded rainfall products (Kumar et al., 2021). Based on the analysis of 18 extreme precipitation events during 2014–16 in the northwest Himalaya (including our study site), however, Jena et al. (2020) conclude that CHIRPS v2 provides the most reliable precipitation estimates. Moreover, the two-peaked rainfall pattern of CHIRPS v2 is most consistent with long-term rainfall patterns obtained from the interpolation of 44 rainfall gauge records averaging over the period from 1901 to 1950 which show highest values along the Himalayan Front and the physiographic transition to the High Himalaya (Basistha et al., 2008; Bookhagen, 2010).

Lithozones derived from a geological map contributed to the explanatory power of the model, thus highlighting the role of lithological properties in modulating landslide susceptibility. As we did not measure the actual geotechnical and -mechanical properties or e.g., bedding and foliation along our route, we can only provide a first order reasoning of the prediction capacity of the lithozones. The high landslide density in lithozone 2 is likely related due to the pronounced fissility and cleavage of the dominating shales and phyllites associated with material softening, percolation and weathering, causing a general decrease in rock strength. Tectonic activity adds to a general decrease in rock strength by creating shear surfaces with low friction angles (Stead, 2016). In addition, road segments, where the adjoining hillslopes parallel bedding, joints or foliation planes are particularly vulnerable (e.g., Bartarya and Valdiya, 1989). Conversely, lithozone 4 is characterized by quartzite and igneous rocks. These have undergone low- to high-grade metamorphism and are generally harder and have a more irregular fabric that restrains the formation of planar slide surfaces. Moreover these rocks tend to develop more stable regolith mantles (Gerrard, 1994), and are thus less susceptible to landsliding. Our model shows that under same topographic conditions and rainfall amounts, the rock types of lithozone 2 are 2–6 times more susceptible to landslides than those in lithozone 4 (Figure 6c). The remaining lithozones are not credibly different from each other, which can partly be attributed to the small fraction of road distance along them (Table 2). Notwithstanding, a general trend towards lower landslide susceptibility from lithozone 1–5 are consistent with a previous review study about lithological controls on the occurrence of mass movements in the Himalaya (Gerrard, 1994).

Our model may miss important predictor variables that control the occurrence of landslides. We included variables that characterize environmental conditions and found that slope, rainfall and lithology largely explain the variability in landslide density. Variables such as landuse or topographic derivatives do not improve the performance of the model as measured by the AIC. Yet, previous studies indicate that human activities have played a crucial role in predisposing slopes to failure (Li et

https://doi.org/10.5194/nhess-2022-295
Preprint. Discussion started: 10 January 2023

Natural Hazards and Earth System Sciences
Discussions

al., 2020; van Westen et al., 2008). The map in Sati et al. (2011) indicates an intriguing spatial agreement between recent constructions for road widenings and landslide occurrences in our study region. The road was widened by removing vegetation and excavating soil and rocks, potentially creating unstable slopes (Barnard et al., 2001; Haigh & Rawat, 2011; Sati et al., 2011; Li et al., 2020). In fact, these disturbances have led to frequent landslides along the NH-7 previously as Sati et al. (2011) also report about ~300 landslides occurring along the road more than 10 years ago. Our data indicates that 20–40 % of the recorded landslides are reactivated slope failures which underscores that slopes are recurrently unstable during periods with intense rainfall (Joshi and Kumar, 2006). During mapping, we also noticed that some slopes were engineered during the last years with retaining walls, yet many of which also failed.

Our model hindcasts the spatial pattern of road-blocking landslides and we posit that it can be used as time-predictive model as well. Rainfall is one of the main covariates in the model and is also the one with the largest uncertainties as shown by the discrepancies of gridded rainfall products. A denser network of rain gauges and a better availability of this data would likely contribute, together with weather forecasting, to more accurate estimates of landslide occurrences which ultimately would facilitate a more efficient allocation of resources for road maintenance. Also, recurrent slope failures should be monitored more closely to direct efforts for slope reinforcements. The land cover data, which we included in the model, is too coarse to capture the widespread lack of vegetation along the road. As many of the landslides were shallow, revegetating slopes may contribute to their stabilization.

To this end, the NH-7 is a key arterial road and landslides make transport of goods and people difficult thus causing serious economic disruption. Moreover, slope failures along the road have led to fatalities in parts where roads were widened. Damages and fatalities may become even more frequent in the future. The entire Upper Ganga basin is susceptible to extreme rainfall events (Joshi and Kumar, 2006), and climate change projections – although subject to high uncertainties – indicate a trend towards more frequent extreme events due to elevation-dependent warming and a likely increase of summer monsoon precipitation by 4–25 % (Krishnan et al., 2019). In addition, exposure to landslides is likely to increase. Road construction and increased traffic volumes attract more people, who will strive for new economic opportunities associated with roadside sites (Fort et al., 2010). These sites are often more susceptible to landslides as construction often implies vegetation removal and slope destabilization (Petley et al., 2007, Li et al., 2020). A reduction of traffic may disrupt the cycle of increasing hazard and exposure. The commissioning of the currently constructed 125 km long broad-gauge railway between Rishikesh and Karnprayag (Azad et al., 2022) might be an important step towards this goal.

6 Conclusions

Road construction is soaring in the Himalayas. During the last five years, ~11,000 km road were built in the Indian Himalayan states (The Tribune, 2022). Yet, the fragility of the Himalayan landscape as well as slope undercutting and poor construction practices make maintenance of these roads challenging. Our study of landslides along the NH-7 demonstrates the scale of this challenge as we detect more than one partially or fully road-blocking landslide per road kilometer between Rishikesh and Joshimath. We contribute to a better understanding and prediction of these landslides by the mapping of a landslide inventory and the adoption of a novel approach to landslide susceptibility analysis which treats the landslides as unmarked network-attached spatial point phenomena. Together with inhomogeneous Poisson process models, this inventory enables us to identify the main controlling variables, i.e. slope angle, rainfall amount and lithology. Further development could potentially involve a conceptualization of landslides as marked point process by incorporation of additional attributes, e.g. landslide size classes. Because of the reduction of the amount of required data, the method can be extended to more complicated road networks with larger spatial extents, while maintaining a high spatial detail and computational efficiency.

Code and data availability. The code and data to run the analysis are available in the supplemental data.

Author contributions. All authors conceived the study and conducted mapping landslides. RKG retrieved and analyzed the rainfall data. JM and AP compiled, analyzed and visualized the data and WS conducted the statistical analysis. All authors wrote the manuscript.

Competing interests. The authors declare that they have no conflict of interest.

Acknowledgments. We acknowledge the German Exchange Service (DAAD) for funding the project Co-PREPARE (Project-ID: 57553291), a joint project of the IIT Roorkee and University of Potsdam. JM acknowledges financial support from the Research Focus "Earth and Environmental Systems" of the University of Potsdam. RKG acknowledges the financial support received from the Prime Minister's Research Fellowship, Government of India for Grant number PM-31-22-695-414.

References

Adhikari, D., Tiwary, R., Singh, P. P., Suchiang, B. R., Nonghuloo, I. M., and Barik, S. K.: Trees, Shrubs and Herbs for Slope Stabilization in Landslide Prone Areas of Eastern Himalaya BT - Nature-based Solutions for Resilient Ecosystems and Societies, edited by: Dhyani, S., Gupta, A. K., and Karki, M., Springer Singapore, Singapore, 307–326, https://doi.org/10.1007/978-981-15-4712-6_18, 2020.

Andermann, C., Bonnet, S., and Gloaguen, R.: Evaluation of precipitation data sets along the Himalayan front, Geochemistry, Geophys. Geosystems, 12, https://doi.org/10.1029/2011GC003513, 2011.

Ang, Q., Baddeley, A., and Nair, G.: Geometrically Corrected Second Order Analysis of Events on a Linear Network, with Applications to Ecology and Criminology, Scand. J. Stat., 39, 591–617, https://doi.org/10.1111/j.1467-9469.2011.00752.x, 2012.

Asthana, B. N. and Khare, D.: Hill Slope Stabilization at Dam and Power Projects in Himalayas BT - Recent Advances in Dam Engineering, edited by: Asthana, B. N. and Khare, D., Springer International Publishing, Cham, 239–264, https://doi.org/10.1007/978-3-030-32278-6_11, 2022.

Azad, M. A., Singh, S. K., Alok, A., Meenakshi, Shekhar, S., and Kumar, P.: Geotechnical and geological studies of Adit-6 of the railway tunnel between Rishikesh and Karnprayag in India focusing on the excavation methods and design of support analysis: a case study, Arab. J. Geosci., 15, 129, https://doi.org/10.1007/s12517-021-09355-7, 2022.

Baddeley, A., Nair, G., Rakshit, S., McSwiggan, G., and Davies, T. M.: Analysing point patterns on networks — A review, Spat. Stat., 42, 100435, https://doi.org/10.1016/J.SPASTA.2020.100435, 2021.

Baddeley, A., Rubak, E., and Turner, R.: Spatial point patterns: methodology and applications with R, CRC press, 2015.

Barnard, P. L., Owen, L. A., Sharma, M. C., and Finkel, R. C.: Natural and human-induced landsliding in the Garhwal Himalaya of northern India, Geomorphology, 40, 21–35, https://doi.org/10.1016/S0169-555X(01)00035-6, 2001.

Bartarya, S. K. and Valdiya, K. S.: Landslides and Erosion in the Catchment of the Gaula River, Kumaun Lesser Himalaya, India, Mt. Res. Dev., 9, 405, 1989.

Basistha, A., Arya, D. S., and Goel, N. K.: Spatial Distribution of Rainfall in Indian Himalayas – A Case Study of Uttarakhand Region, Water Resour. Manag., 22, 1325–1346, https://doi.org/10.1007/s11269-007-9228-2, 2008.

Beck, H. E., Vergopolan, N., Pan, M., Levizzani, V., van Dijk, A. I. J. M., Weedon, G. P., Brocca, L., Pappenberger, F., Huffman, G. J., and Wood, E. F.: Global-scale evaluation of 22 precipitation datasets using gauge observations and hydrological modeling, Hydrol. Earth Syst. Sci., 21, 6201–6217, https://doi.org/10.5194/hess-21-6201-2017, 2017.

Bollinger, L., Sapkota, S. N., Tapponnier, P., Klinger, Y., Rizza, M., Van der Woerd, J., Tiwari, D. R., Pandey, R., Bitri, A., and Bes de Berc, S.: Estimating the return times of great Himalayan earthquakes in eastern Nepal: Evidence from the Patu and Bardibas strands of the Main Frontal Thrust, J. Geophys. Res. Solid Earth, 119, 7123–7163, https://doi.org/10.1002/2014JB010970, 2014.

Bookhagen, B.: Appearance of extreme monsoonal rainfall events and their impact on erosion in the Himalaya, Geomatics, Nat. Hazards Risk, 1, 37–50, https://doi.org/10.1080/19475701003625737, 2010.

Buchhorn, M., Smets, B., Bertels, L., Roo, B. De, Lesiv, M., Tsendbazar, N.-E., Li, L., and Tarko, A.: Copernicus Global Land Service: Land Cover 100m: version 3 Globe 2015-2019: Product User Manual, https://doi.org/10.5281/zenodo.3938963, 2020.

Das, I., Stein, A., Kerle, N., and Dadhwal, V. K.: Landslide susceptibility mapping along road corridors in the Indian Himalayas using Bayesian logistic regression models, Geomorphology, 179, 116–125, https://doi.org/10.1016/j.geomorph.2012.08.004, 2012.

Devkota, K. C., Regmi, A. D., Pourghasemi, H. R., Yoshida, K., Pradhan, B., Ryu, I. C., Dhital, M. R., and Althuwaynee, O. F.: Landslide susceptibility mapping using certainty factor, index of entropy and logistic regression models in GIS and their comparison at Mugling–Narayanghat road section in Nepal Himalaya, Nat. Hazards, 65, 135–165, https://doi.org/10.1007/s11069-012-0347-6, 2013.

European Space Agency, Sinergise. Copernicus Global Digital Elevation Model. Distributed by OpenTopography, Accessed: 2022-12-27, https://doi.org/10.5069/G9028PQB, 2021.

Evans, I. S.: Geomorphometry and landform mapping: What is a landform?, Geomorphology, 137, 94–106, https://doi.org/10.1016/j.geomorph.2010.09.029, 2012.

Fort, M., Cossart, E., and Arnaud-Fassetta, G.: Hillslope-channel coupling in the Nepal Himalayas and threat to man-made structures: The middle Kali Gandaki valley, Geomorphology, 124, 178–199, https://doi.org/https://doi.org/10.1016/j.geomorph.2010.09.010, 2010.

Funk, C., Peterson, P., Landsfeld, M., Pedreros, D., Verdin, J., Shukla, S., Husak, G., Rowland, J., Harrison, L., Hoell, A., and Michaelsen, J.: The climate hazards infrared precipitation with stations—a new environmental record for monitoring extremes, Sci. Data, 2, 150066, https://doi.org/10.1038/sdata.2015.66, 2015.

Geological Survey of India: Uttarakhand lithology, Government of India, Kolkata, India, 08.10.2022, https://bhukosh.gsi.gov.in, 2022.

Gerrard, J.: The landslide hazard in the Himalayas: geological control and human action, edited by: Morisawa, M. B. T.-G. and N. H., Elsevier, Amsterdam, 221–230, https://doi.org/10.1016/B978-0-444-82012-9.50019-0, 1994.

Haigh, M. J.: Landslide prediction and highway maintenance in the Lesser Himalaya, India, Zeitschrift für Geomorphol. Suppl., 51, 17–38, 1984.

Haigh, M. and Rawat, J. S.: Landslide causes : Human impacts on a Himalayan landslide swarm, Belgian J. Geogr., 3–4, 201–220, https://doi.org/10.4000/belgeo.6311, 2011.

Hu, Z., Hu, Q., Zhang, C., Chen, X., and Li, Q.: Evaluation of reanalysis, spatially interpolated and satellite remotely sensed precipitation data sets in central Asia, J. Geophys. Res. Atmos., 121, 5648–5663, https://doi.org/10.1002/2016JD024781, 2016.

Jena, P., Garg, S., and Azad, S.: Performance Analysis of IMD High-Resolution Gridded Rainfall (0.25° × 0.25°) and Satellite Estimates for Detecting Cloudburst Events over the Northwest Himalayas, J. Hydrometeorol., 21, 1549–1569, https://doi.org/10.1175/JHM-D-19-0287.1, 2020.

Joshi, V. and Kumar, K.: Extreme rainfall events and associated natural hazards in Alaknanda valley, Indian Himalayan region, J. Mt. Sci., 3, 228–236, https://doi.org/10.1007/s11629-006-0228-0, 2006.

Kanungo, D. P., Pain, A., and Sharma, S.: Finite element modeling approach to assess the stability of debris and rock slopes: a case study from the Indian Himalayas, Nat. Hazards, 69, 1–24, https://doi.org/10.1007/s11069-013-0680-4, 2013.

Kayal, J. R., Ram, S., Singh, O. P., Chakraborty, P. K., and Karunakar, G.: Aftershocks of the March 1999 Chamoli Earthquake and Seismotectonic Structure of the Garhwal Himalaya, Bull. Seismol. Soc. Am., 93, 109–117, 2003.

Koushik, P., Shantanu, S., Manojit, S., and Mahesh, S.: Stability analysis and design of slope reinforcement techniques for a Himalayan landslide BT - Proceedings of the conference on Recent Advances in Rock Engineering (RARE 2016), 97–104, https://doi.org/10.2991/rare-16.2016.16, 2016.

Krishnan, R., Shrestha, A. B., Ren, G., Rajbhandari, R., Saeed, S., Sanjay, J., Syed, M. A., Vellore, R., Xu, Y., You, Q., and Ren, Y.: Unravelling Climate Change in the Hindu Kush Himalaya: Rapid Warming in the Mountains and Increasing Extremes - The Hindu Kush Himalaya Assessment: Mountains, Climate Change, Sustainability and People, edited by: Wester, P., Mishra, A., Mukherji, A., and Shrestha, A. B., Springer International Publishing, Cham, 57–97, https://doi.org/10.1007/978-3-319-92288-1_3, 2019.

Kubota, T., Shige, S., Hashizume, H., Aonashi, K., Takahashi, N., Seto, S., Hirose, M., Takayabu, Y. N., Ushio, T., Nakagawa, K., Iwanami, K., Kachi, M., and Okamoto, K.: Global Precipitation Map Using Satellite-Borne Microwave Radiometers by the GSMaP Project: Production and Validation, IEEE Trans. Geosci. Remote Sens., 45, 2259–2275, https://doi.org/10.1109/TGRS.2007.895337, 2007.

Kumar, M., Hodnebrog, Ø., Sophie Daloz, A., Sen, S., Badiger, S., and Krishnaswamy, J.: Measuring precipitation in Eastern Himalaya: Ground validation of eleven satellite, model and gauge interpolated gridded products, J. Hydrol., 599, 126252, https://doi.org/10.1016/j.jhydrol.2021.126252, 2021.

Kundu, J., Sarkar, K., and Singh, A. K.: Integrating structural and numerical solutions for road cut slope stability analysis-a case study, India, in: ISRM 2nd International Conference on Rock Dynamics, 2016.

Lave, J. and Avouac, J. P.: Fluvial incision and tectonic uplift across the Himalayas of central Nepal, J. Geophys. Res., 106, 2001.

Li, Y., Wang, X., and Mao, H.: Influence of human activity on landslide susceptibility development in the Three Gorges area, Nat. Hazards, 104, 2115–2151, https://doi.org/10.1007/s11069-020-04264-6, 2020.

Lombardo, L., Bakka, H., Tanyas, H., van Westen, C., Mai, P. M., and Huser, R.: Geostatistical Modeling to Capture Seismic-Shaking Patterns From Earthquake-Induced Landslides, J. Geophys. Res. Earth Surf., 124, 1958–1980, https://doi.org/10.1029/2019JF005056, 2019.

Lombardo, L., Opitz, T., and Huser, R.: Point process-based modeling of multiple debris flow landslides using INLA: an application to the 2009 Messina disaster, Stoch. Environ. Res. Risk Assess., 32, 2179–2198, https://doi.org/10.1007/s00477-018-1518-0, 2018.

Makalic, E. and Schmidt, D. F.: A Simple Bayesian Algorithm for Feature Ranking in High Dimensional Regression Problems. AI 2011: Advances in Artificial Intelligence, 223–230, 2011.

Makalic, E. and Schmidt, D. F.: High-Dimensional Bayesian Regularised Regression with the BayesReg Package, arXiv. https://doi.org/10.48550/ARXIV.1611.06649, 2016.

Meyer, N. K., Schwanghart, W., Korup, O., and Nadim, F.: Roads at risk: traffic detours from debris flows in southern Norway, Nat. Hazards Earth Syst. Sci., 15, 985–995, https://doi.org/10.5194/nhess-15-985-2015, 2015.

Mitra, A. K., Bohra, A. K., Rajeevan, M. N., and Krishnamurti, T. N.: Daily Indian Precipitation Analysis Formed from a Merge of Rain-Gauge Data with the TRMM TMPA Satellite-Derived Rainfall Estimates, J. Meteorol. Soc. Japan. Ser. II, 87A, 265–279, https://doi.org/10.2151/jmsj.87A.265, 2009.

National Crime Records Bureau: Accidental Deaths & Suicides in India 2021, https://ncrb.gov.in/en/node/3722, 2022.

Okabe, A., Okunuki, K., and Shiode, S.: SANET: A Toolbox for Spatial Analysis on a Network, Geogr. Anal., 38, 57–66, https://doi.org/10.1111/j.0016-7363.2005.00674.x, 2006.

Okabe, A. and Sugihara, K.: Spatial analysis along networks: statistical and computational methods, John Wiley & Sons, 2012.

Ozturk, U., Saito, H., Matsushi, Y., Crisologo, I., and Schwanghart, W.: Can global rainfall estimates (satellite and reanalysis) aid landslide hindcasting?, Landslides, 18, 3119–3133, https://doi.org/10.1007/s10346-021-01689-3, 2021.

Pai, D. S., Sridhar, L., Rajeevan, M., Sreejith, O. P., Satbhai, N. S., and Mukhopadhyay, B.: Development of a new high spatial resolution (0.25° × 0.25°) long period (1901-2010) daily gridded rainfall data set over India and its comparison with existing data sets over the region, MAUSAM, 1, 1–18, https://doi.org/10.54302/mausam.v65i1.851, 2014.

Petley, D. N., Hearn, G. J., Hart, A., Rosser, N. J., Dunning, S. A., Oven, K., and Mitchell, W. A.: Trends in landslide occurrence in Nepal, Nat. Hazards, 43, 23–44, https://doi.org/10.1007/s11069-006-9100-3, 2007.

Prasad, S. and Siddique, T.: Stability assessment of landslide-prone road cut rock slopes in Himalayan terrain: A finite element method based approach, J. Rock Mech. Geotech. Eng., 12, 59–73, https://doi.org/10.1016/j.jrmge.2018.12.018, 2020.

Rajendran, K., Parameswaran, R. M., and Rajendran, C. P.: Seismotectonic perspectives on the Himalayan arc and contiguous areas: Inferences from past and recent earthquakes, Earth-Science Rev., 173, 1–30, https://doi.org/10.1016/j.earscirev.2017.08.003, 2017.

Rawat, M. S., Joshi, V., Uniyal, D. P., and Rawat, B. S.: Investigation of hill slope stability and mitigation measures in Sikkim Himalaya, Int. J. Landslide Environ., 3, 8–15, 2016.

Sarkar, S. and Kanungo, D. P.: Landslides in the Alaknanda Valley of Garhwal Himalaya, India, Q. J. Eng. Geol. Hydrogeol., 39, 79–82, https://doi.org/10.1144/1470-9236/05-020, 2006.

Sati, S. P., Sundriyal, Y., Rana, N., and Dangwal, S.: Recent landslides in Uttarakhand: nature’s fury or human folly, Curr. Sci., 100, 2011.

Schwanghart, W. and Scherler, D.: Bumps in river profiles: uncertainty assessment and smoothing using quantile regression techniques, Earth Surf. Dyn., 5, 821–839, https://doi.org/10.5194/esurf-5-821-2017, 2017.

Schwanghart, W. and Scherler, D.: Short Communication: TopoToolbox 2 – MATLAB-based software for topographic analysis and modeling in Earth surface sciences, Earth Surf. Dyn., 2, 1–7, https://doi.org/10.5194/esurf-2-1-2014, 2014.

Schwanghart, W., Molkenthin, C., and Scherler, D.: A systematic approach and software for the analysis of point patterns on river networks, Earth Surf. Process. Landforms, 46, 1847–1862, https://doi.org/10.1002/esp.5127, 2021.

Shugar, D. H., Jacquemart, M., Shean, D., Bhushan, S., Upadhyay, K., Sattar, A., Schwanghart, W., McBride, S., van Wyk de Vries, M., Mergili, M., Emmer, A., Deschamps-Berger, C., McDonnell, M., Bhambri, R., Allen, S., Berthier, E., Carrivick, J. L., Clague, J. J., Dokukin, M., Dunning, S. A., Frey, H., Gascoin, S., Haritashya, U. K., Huggel, C., Kääb, A., Kargel, J. S., Kavanaugh, J. L., Lacroix, P., Petley, D., Rupper, S., Azam, M. F., Cook, S. J., Dimri, A. P., Eriksson, M., Farinotti, D., Fiddes, J., Gnyawali, K. R., Harrison, S., Jha, M., Koppes, M., Kumar, A., Leinss, S., Majeed, U., Mal, S., Muhuri, A., Noetzli, J., Paul, F., Rashid, I., Sain, K., Steiner, J., Ugalde, F., Watson, C. S., and Westoby, M. J.: A massive rock and ice avalanche caused the 2021 disaster at Chamoli, Indian Himalaya, Science, 373, 300–306, https://doi.org/10.1126/science.abh4455, 2021.

Siddique, T. and Pradhan, S. P.: Stability and sensitivity analysis of Himalayan road cut debris slopes: an investigation along NH-58, India, Nat. Hazards, 93, 577–600, https://doi.org/10.1007/s11069-018-3317-9, 2018.

Siddique, T., Pradhan, S. P., Vishal, V., Mondal, M. E. A., and Singh, T. N.: Stability assessment of Himalayan road cut slopes along National Highway 58, India, Environ. Earth Sci., 76, 1–18, 2017.

Singh, R., Umrao, R. K., and Singh, T. N.: Stability evaluation of road-cut slopes in the Lesser Himalaya of Uttarakhand, India: conventional and numerical approaches, Bull. Eng. Geol. Environ., 73, 845–857, 2014.

Stanley, T. and Kirschbaum, D. B.: A heuristic approach to global landslide susceptibility mapping, Nat. Hazards, 87, 145–164, https://doi.org/10.1007/s11069-017-2757-y, 2017.

Stead, D.: The Influence of Shales on Slope Instability, Rock Mech. Rock Eng., 49, 635–651, https://doi.org/10.1007/s00603-015-0865-0, 2016.

Sur, U., Singh, P., and Meena, S. R.: Landslide susceptibility assessment in a lesser Himalayan road corridor (India) applying fuzzy AHP technique and earth-observation data, Geomatics, Nat. Hazards Risk, 11, 2176–2209, https://doi.org/10.1080/19475705.2020.1836038, 2020.

Swarnkar, S., Mujumdar, P., and Sinha, R.: Modified hydrologic regime of upper Ganga basin induced by natural and anthropogenic stressors, Sci. Rep., 1–11, https://doi.org/10.1038/s41598-021-98827-7, 2021.

The Tribune, India: https://www.tribuneindia.com/news/nation/10-969-km-roads-in-himalayan-states-461738, last access: 29 December 2022.

United States Geological Survey (USGS), Earthquake Catalog, https://earthquake.usgs.gov/earthquakes/search/, last access: 27 November 2022.

Uniyal, A.: Infra Development Vision for Himalaya in the Aftermath of Rishiganga Tragedy, Disaster & Development, 149–159 pp., 2021.

van Westen, C. J., Castellanos, E., and Kuriakose, S. L.: Spatial data for landslide susceptibility, hazard, and vulnerability assessment: An overview, Eng. Geol., 102, 112–131, https://doi.org/10.1016/j.enggeo.2008.03.010, 2008.

Wang, Q., Zhang, P.-Z., Freymueller, J. T., Bilham, R., Larson, K. M., Lai, X., You, X., Niu, Z., Wu, J., Li, Y., Liu, J., Yang, Z., and Chen, Q.: Present-Day Crustal Deformation in China Constrained by Global Positioning System Measurements, Science, 294, 574–577, https://doi.org/10.1126/science.1063647, 2001.

https://doi.org/10.5194/nhess-2022-295
Preprint. Discussion started: 10 January 2023

Figures

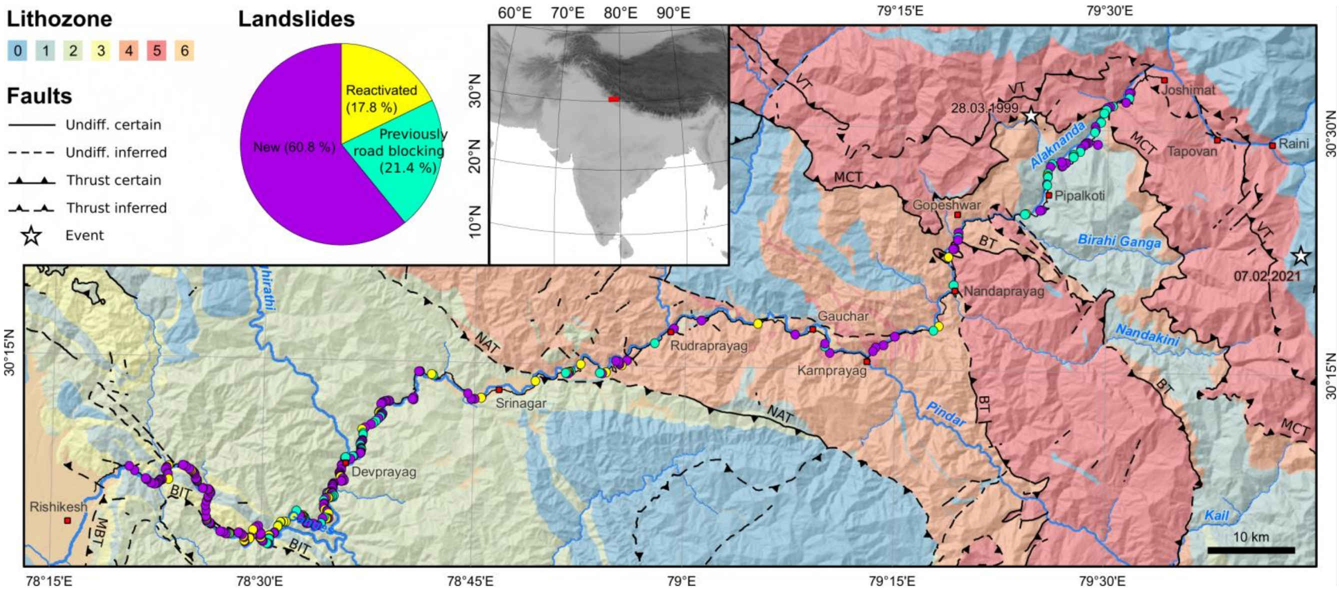

520 **Figure 1: Map of the study site.** Landslides, lithozones and major faults along NH-7 from Rishikesh to Joshimath. The highest density of landslides occurs between Rishikesh and Srinagar within lithozone 2 and between Pipalkoti and Joshimath in lithozone 1. For description of the lithozones see Table 2. Note that lithozones 0 and 6 are not crossed by the road and are therefore omitted from the description. We subdivided the landslides into new ones, reactivated ones and those that were blocking the road before September 2022. Lithozones and faults were modified from digital maps provided by the
525 Geological Survey of India (2022). Stars indicate locations of the 1999 M_w 6.6 Chamoli earthquake (Kayal et al., 2003; USGS, 2022) and the 2021 Chamoli rock and ice avalanche (Shugar et al., 2021). MBT: Main Boundary Thrust, BIT: Bijni Thrust, NAT: North Almora Thrust, BT: Baijnat Thrust, MCT: Main Central Thrust, VT: Vaikrita Thrust.

Figure 2: Examples of partially road-blocking landslides along the highway NH-7. Panels a) and c) show locations, where hillslopes parallel the foliation/bedding.

https://doi.org/10.5194/nhess-2022-295
Preprint. Discussion started: 10 January 2023

Natural Hazards and Earth System Sciences
Open Access
Discussions

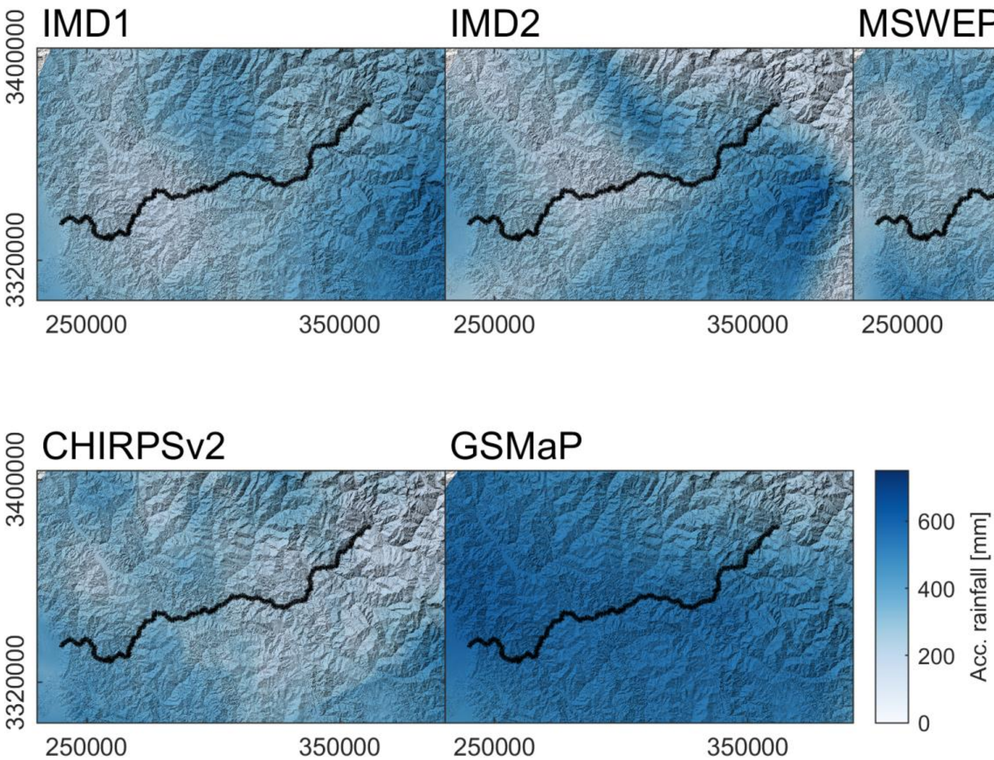

Figure 3: Accumulated rainfall amounts from different rainfall products. The black line indicates the road between Rishikesh and Joshimath (see Fig. 1).

https://doi.org/10.5194/nhess-2022-295
Preprint. Discussion started: 10 January 2023

535

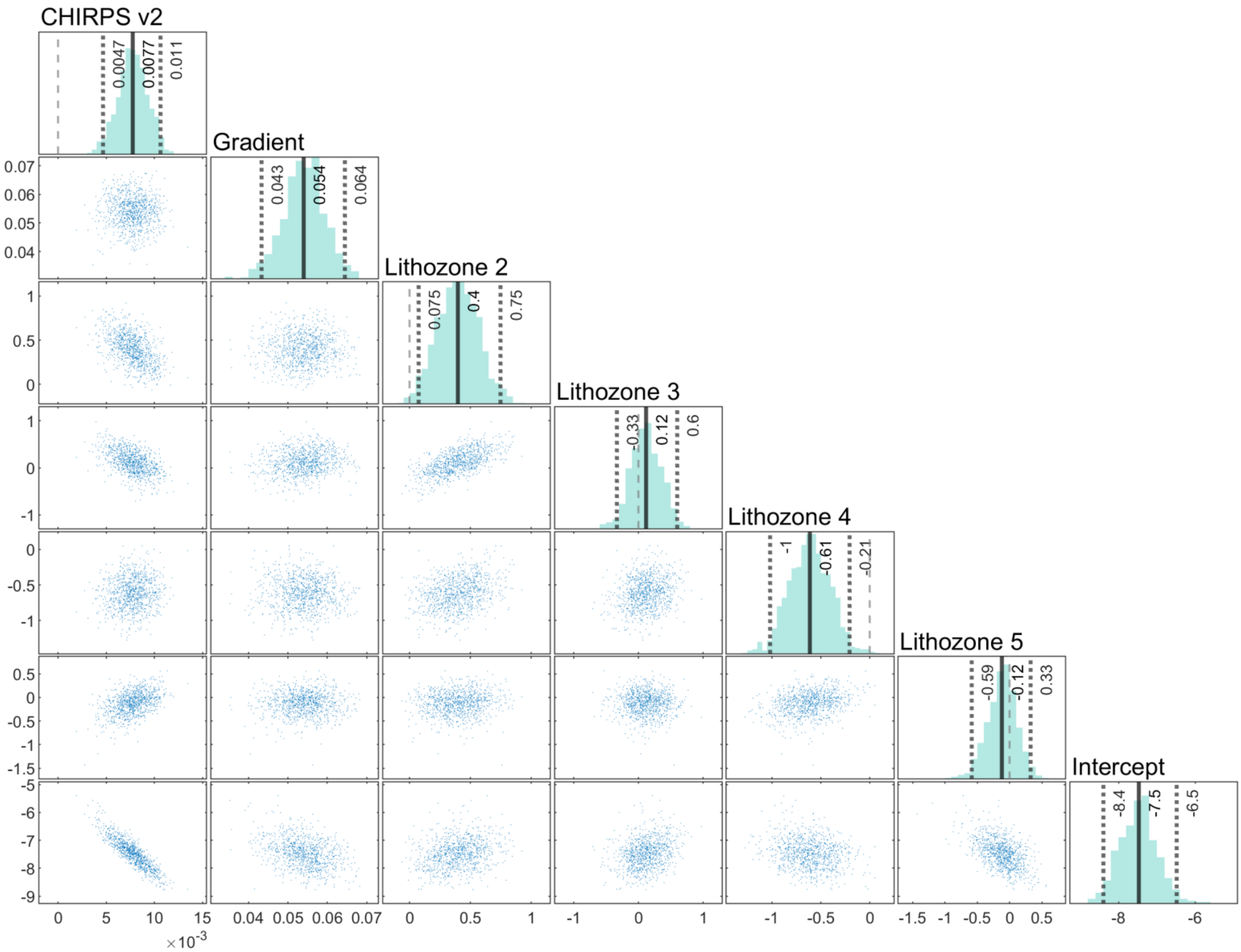

Figure 4: Posterior parameter samples of the loglinear model of landslide occurrence along the NH-7. CHIRPS v2 is the gridded rainfall product, gradient determines the slope within 210 m to the road and lithozones were aggregated from a geological map. Note that Lithozone 1 is missing since the parameter is encapsulated in the intercept.

Natural Hazards and Earth System Sciences
Open Access
Discussions
EGU

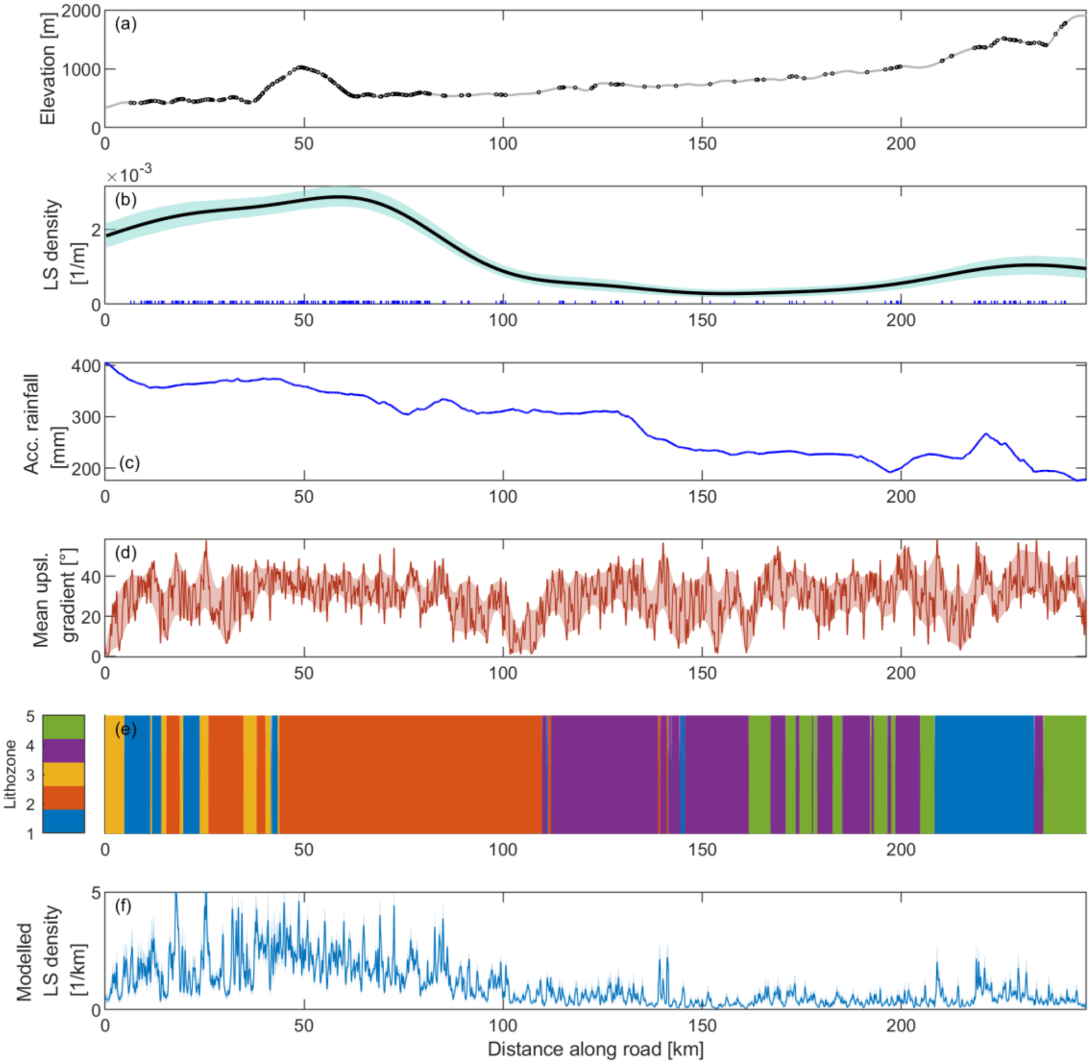

540 **Figure 5: Predictor and response variables used in the model.** a) shows the occurrences of the fully and partially road-blocking landslides together with the elevation profile of the road. b) Landslide density along the road using a Gaussian kernel and 15 km bandwidth as well as bootstrapped confidence bounds. c) Accumulated rainfall during September, 1-30 and October, 1-12, 2022 from CHIRPS v2. d) Mean upslope gradient within a distance of 210 m around the road. The shaded area denotes the 5 and 95 **%** bounds using a nonparametric quantile regression and highlights the larger scale variability of gradient. e) Lithozones along the road (see also Fig. 1). f)
545 Predicted landslide density using a model involving rainfall, slope and lithozones as covariates.

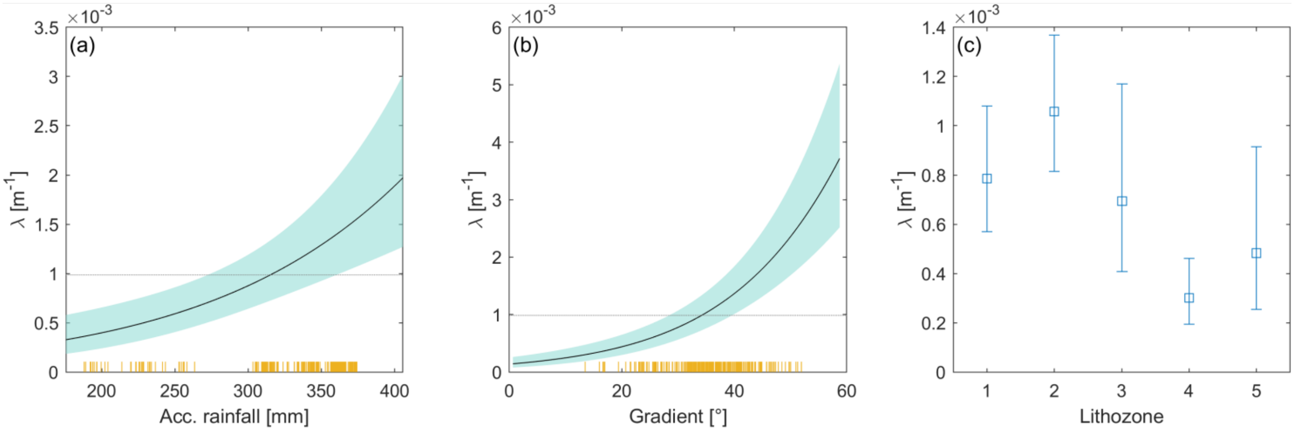

550 **Figure 6: Main effects of predictors in the loglinear model of road-blocking landslides along the NH-7.** a) Effect of accumulated rainfall amount during September, 1-30, and October, 1-12, 2022, on the occurrence of landslides, averaging out the effects of the other predictors. The orange lines indicate the occurrences of landslides. b) Effect of hillslope gradient and c) of lithozone.

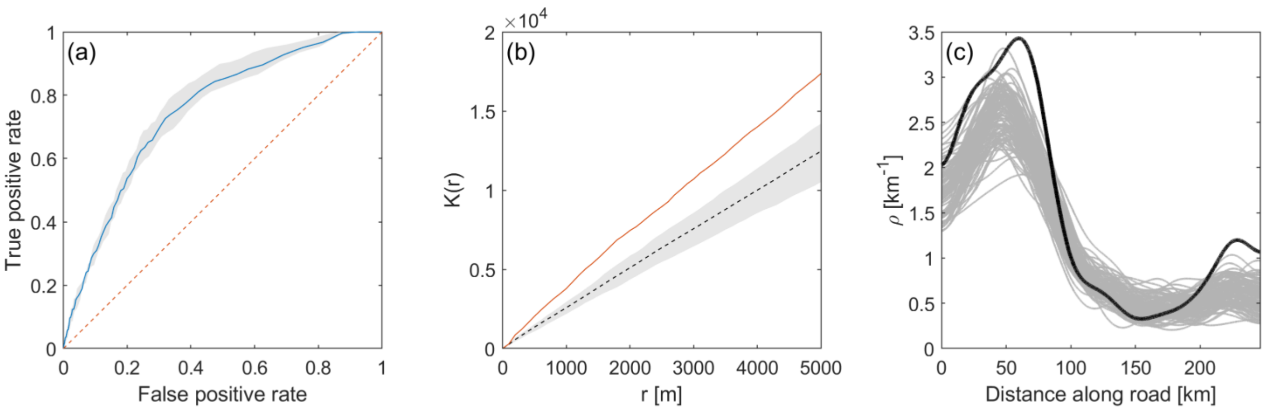

555 **Figure 7: Evaluation of the loglinear model including rainfall, slope and lithozones.** a) Receiver-operating-characteristics (ROC) curve. The area-under-the-curve (AUC) metric is 0.76. b) The inhomogeneous K-function corrects for the influence of an inhomogeneous Poisson point process model and tests for second order effects (e.g., spatial clustering). Acceptance intervals of a theoretical model without point independence are shown in gray. The red line is the empirical inhomogeneous K-function, which indicates clustering. c) Comparison of observed landslide densities (black line) with densities obtained from 100 random realizations (gray lines) from the model.

https://doi.org/10.5194/nhess-2022-295
Preprint. Discussion started: 10 January 2023

Natural Hazards and Earth System Sciences
Discussions

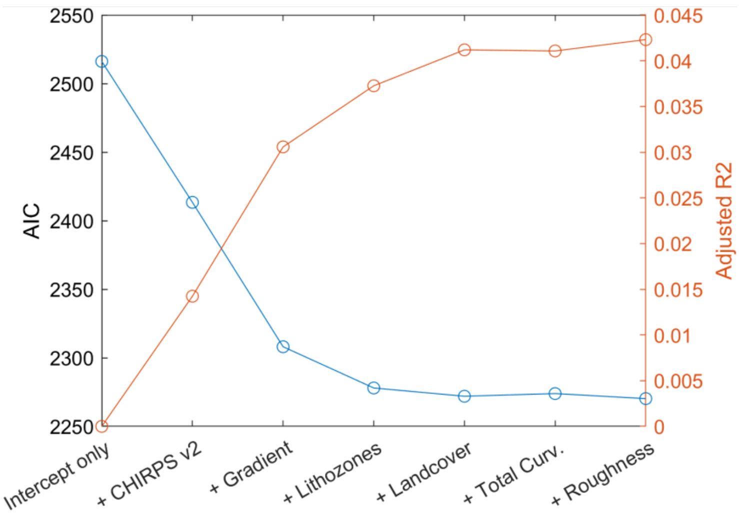

Figure 8: Forward stepwise selection of additional explanatory covariates in the loglinear model of road-blocking landslides.

Tables

Table 1. Overview of the rainfall products.

Product	Full form	Spatial resolution	Link to source	Reference
IMD1	Indian Meteorological Department 1	0.25° x 0.25°	http://www.imdpune.gov.in/Clim_Pred_LRF_New/Grided_Data_Download.html	Pai et al., 2014
IMD2	Indian Meteorological Department 2	0.25° x 0.25°	http://www.imdpune.gov.in/Clim_Pred_LRF_New/Grided_Data_Download.html	Mitra et al., 2009
MSWEP v2	Multi-Source Weighted-Ensemble Precipitation	0.1° x 0.1°	http://www.gloh2o.org/	Beck et al., 2017
CHIRPS v2	Climate Hazards group Infrared Precipitation with Stations	0.05° x 0.05°	ftp://chg-ftpout.geog.ucsb.edu/pub/org/chg/products/CHIRPS-2.0/	Funk et al., 2015
GSMaP	Global Satellite Mapping of Precipitation	0.1° x 0.1°	https://sharaku.eorc.jaxa.jp/GSMaP_NOW/index.htm	Kubota et al., 2007

Table 2. Definition of lithozones.

Lithozone	Aggregated lithologies	Id	Percentage of road
1	limestone, dolomitic limestone with shale	2072	17 %
	shale with lenticles of limestone	2073	
	argillaceous limestone and clay	2074	
	limestone, dolomite, shale, carb. phyllite/slate	2480	
	limestone	2457	
	dolomite	2456	
2	shale, quartzite, limestone and conglomerate	2109	33 %
	phyllite, qtz, shale, dolomite, tuff with dolerite	2108	
	splintery shale with nodular limestone	746	
	massive sandy limestone	1799	
	limestone, dolomite, shale and cherty quartzite	2482	
	quartzite, slate, lensoidal limestone and tuff	2486	
	massive sandy limestone	1799	
3	quartzite, limestone and occassional conglomerate	1943	6 %
	quartzite, siltstone, chert and phosphatic shale	1944	
	diamictite, quartzite, slate and boulder bed	2081	
	carbonaceous shale, slate, greywacke	2078	
4	quartzite and slate with basic metavolcanics	2464	30 %
	basic meta-volcanics	2458	
	basic / intermediate intrusive	2453	
	porphyritic nonfoliated granite	2452	
5	sericite quartz schist, chlorite schist	2463	14 %
	chlorite schist, hornblende-albite-zoisite schist	2461	
	phyllite with chloritic, graphitic & carbonaceous	2462	
	schist, augen gneiss, quartzite & amphibolite	3702	
	quartz-sericite-chlorite schist & limestone	3701	
	schist, gneiss, marble and basic intrusives	3747	
	gneiss, kyanite schist, quartzite, calc-silicate	3752	
	quartzite and quartz mica schist	3744	
	calc silicate, quartzite, schist, marble band	3743	

[a]Id refers to the UID given in the original data (Geological Survey of India, 2022)

https://doi.org/10.5194/nhess-2022-295
Preprint. Discussion started: 10 January 2023

Table 3. Aggregation of land cover classes derived from the Copernicus Global Land Service version 3 Globe 2015-2019. Remaining map codes in the original data were not concerned along the NH-7.

Aggregated land cover class	**Map codes**
Closed forest	111-116
Open forest	121-126
Shrubland	20, 30
Cropland	40
Built-up	50